

Particle backscatter and relative humidity

M. Brabec et al.

Particle backscatter and relative humidity measured across cirrus clouds and comparison with state-of-the-art cirrus modelling

M. Brabec¹, F. G. Wienhold¹, B. Luo¹, H. Vömel², F. Immler², P. Steiner³, and T. Peter¹

¹Institute for Atmospheric and Climate Science, ETH, Zurich, Switzerland

²Deutscher Wetterdienst, Meteorologisches Observatorium Lindenberg, Germany

³Federal Office of Meteorology and Climatology MeteoSwiss, Switzerland

Received: 23 March 2012 – Accepted: 23 March 2012 – Published: 13 April 2012

Correspondence to: F. G. Wienhold (frank.wienhold@env.ethz.ch)

Published by Copernicus Publications on behalf of the European Geosciences Union.

Title Page

Abstract

Introduction

Conclusions

References

Tables

Figures

◀

▶

◀

▶

Back

Close

Full Screen / Esc

Printer-friendly Version

Interactive Discussion



Abstract

Advanced measurement and modelling techniques are employed to determine the partitioning of atmospheric water between the gas phase and the condensed phase in and around cirrus clouds, and thus to identify in-cloud and out-of-cloud supersaturations with respect to ice. In November 2008 the newly developed balloon-borne backscatter sonde COBALD (Compact Optical Backscatter and Aerosol Detector) was flown 14 times together with a CFH (Cryogenic Frost point Hygrometer) from Lindenberg, Germany (52° N, 14° E). The case discussed here in detail shows two cirrus layers with in-cloud relative humidities with respect to ice between 50 % and 130 %. Global operational analysis data of ECMWF (roughly 1° × 1° horizontal and 1 km vertical resolution, 6-hourly stored fields) fail to represent ice water contents and relative humidities. Conversely, regional COSMO-7 forecasts (6.6 km × 6.6 km, 5-min stored fields) capture the measured humidities and cloud positions remarkably well. The main difference between ECMWF and COSMO data is the resolution of small-scale vertical features responsible for cirrus formation. Nevertheless, ice water contents in COSMO-7 are still off by factors 2–10, likely reflecting limitations in COSMO's ice phase bulk scheme. Significant improvements can be achieved by comprehensive size-resolved microphysical and optical modelling along backward trajectories based on COSMO-7 wind and temperature fields, which allow accurate computation of humidities, ice particle size distributions and backscatter ratios at the COBALD wavelengths. However, only by superimposing small-scale temperature fluctuations, which remain unresolved by the NWP models, can we obtain a satisfying agreement with the observations and reconcile the measured in-cloud non-equilibrium humidities with conventional ice cloud microphysics.

Particle backscatter and relative humidity

M. Brabec et al.

Title Page

Abstract

Introduction

Conclusions

References

Tables

Figures

◀

▶

◀

▶

Back

Close

Full Screen / Esc

Printer-friendly Version

Interactive Discussion



1 Introduction

Water vapour is a key element in the Earth's climate, weather and atmospheric chemistry. Dehydration mechanisms driven by the formation of visible and subvisible cirrus clouds, determine the atmospheric water vapour budget and thus the chemical and radiative properties of the upper troposphere and stratosphere. Though still uncertain, the role of cirrus clouds is of particular importance in the Earth's climate system due to their poorly characterized radiative properties and microphysics (Christensen et al., 2007). Approximately 30 % of the Earth is covered with cirrus clouds, which influence the radiative budget by altering both the reflectivity for incoming solar radiation and the emission of outgoing infrared radiation (Joos et al., 2008). These characteristics motivate cirrus cloud studies.

At times surprisingly high supersaturations inside and around cirrus clouds have been measured, as if the nucleation of ice particles or the uptake of water onto the existing ice surfaces were hindered (Peter et al., 2006, and references therein). Most of these observations have been performed onboard of aircraft. Therefore, a search for similar conditions by means of a different platform is a goal within this study, which describes soundings that were part of the "Lindenberg Upper-Air Methods Intercomparison" (LUAMI, 2008), whose aim was to investigate instrumentation for cirrus cloud measurements in the midlatitude upper troposphere. This campaign took place at the meteorological observatory (52.21° N, 14.12° E) at Lindenberg, Germany. In the present case study we focus on a sounding on 6 November 2008 with profiles of water vapour and particle backscatter measured by the Cryogenic Frost point Hygrometer (CFH) and the newly developed backscatter sonde (COBALD), respectively. These data are evaluated in the present analysis, and the COBALD-CFH tandem is shown to be an excellent payload for cirrus measurements.

CFH provides accurate measurements at cirrus altitudes (Vömel et al., 2007; Möhler et al., 2009). One of the shortcomings of previous radiosonde data is the lack of knowledge whether the measurements took place in clear sky or in cirrus clouds (Spichtinger

Particle backscatter and relative humidity

M. Brabec et al.

Title Page

Abstract

Introduction

Conclusions

References

Tables

Figures

◀

▶

◀

▶

Back

Close

Full Screen / Esc

Printer-friendly Version

Interactive Discussion



et al., 2005a). COBALD's application as a cloud detector provides this information, proving the backscatter sonde to be an essential tool (Wienhold, 2011). Here we analyze the COBALD-CFH cirrus cloud data by means of a detailed case study. First, we use the measurements to explore the ability of global and regional numerical weather prediction (NWP) models to represent microphysical processes in cold, high cirrus clouds. To this end relative humidities and ice water contents from ECMWF analysis data ($1^\circ \times 1^\circ$ spatial resolution, 6-hourly stored fields) and COSMO-7 forecasts ($6.6\text{ km} \times 6.6\text{ km}$, 5-min stored fields; MeteoSwiss, 2012) are directly compared with the measurements. This is an acid test for these models, given the faint nature of the sub-visible cirrus clouds (optical depths $\tau < 0.03$; Sassen, 2002) investigated here. Second, we apply backward trajectories based on input wind fields obtained from the regional COSMO-7 model with a time resolution of 5 min to force a comprehensive microphysical box and column model (Luo et al., 2003a,b) using the trajectory temperature and pressure data to explore the more detailed cloud properties.

2 Methods: instrumentation, meteorological data and models

This section provides technical information on the COBALD and CFH sondes, on the model data from ECMWF analyses, COSMO-7 forecast runs (Doms et al., 2011) and LAGRANTO, the "LAGRangian ANalysis TOol", a trajectory model (Wernli and Davies, 1997). Finally, the Zurich Optical and Microphysical Model (ZOMM), a state-of-the-art Lagrangian box and column model (Luo et al., 2003a,b) is introduced, which is used to describe the microphysical cirrus processes in full size-resolution.

2.1 COBALD

COBALD is a newly developed lightweight backscatter sonde designed to be flown on operational weather balloons. It is based on similar principles to the Wyoming backscatter sonde of Rosen and Kjome (1991), which has been used extensively in field studies

Particle backscatter and relative humidity

M. Brabec et al.

Title Page

Abstract

Introduction

Conclusions

References

Tables

Figures

◀

▶

◀

▶

Back

Close

Full Screen / Esc

Printer-friendly Version

Interactive Discussion



(e.g., Larsen et al., 1994; Rosen et al., 1997; Beyerle et al., 2001). COBALD uses two high power (250 mW) LEDs at wavelengths centered at 455 nm (blue) and 870 nm (infrared). A silicon detector measures the light backscattered at both wavelengths by air molecules, aerosol particles or cloud droplets and ice particles. The data are analyzed based on the procedure developed by Rosen and Kjome (1991).

The raw backscatter signal comprises two contributions, the molecular (or “Rayleigh”) contribution and the additional aerosol or particulate contribution. The raw signal is normalized to the molecular scattering, derived from the ambient molecular number density, using the temperature and pressure measured by the pTu-sonde. The result is the backscatter ratio (BSR). Accordingly, the aerosol/particle backscatter is defined as $ABSR = BSR - 1$.

Estimated maximum uncertainties in the BSR are about 1.3 % or 5 % in the red channel at ground level or 10 km altitude, respectively, and similarly 0.2 % or 1 % at the same altitudes in the blue channel. This renders a proper characterization of the tropospheric background aerosol difficult. However, an estimate of ABSR of cirrus clouds – even the very thin, subvisible ones – is hardly affected by these errors, yielding a maximum error of 10 % (for $ABSR = 1$ in the red channel).

2.2 Cryogenic Frost point Hygrometer (CFH)

The CFH was developed at the University of Colorado (Vömel et al., 2007) and defines the state-of-the-art measurement technology for atmospheric water vapour. Its design is based on the older NOAA/CMDL frost point hygrometer, with improved accuracy. Frost point hygrometers operate by cooling a mirror, which is controlled with an opto-electronic feedback to maintain a constant layer of liquid or frozen condensate. The mirror temperature corresponds to the dew or frost point temperature ($T_{\text{mirror}} = T_{\text{dew}}$ or $T_{\text{mirror}} = T_{\text{ice}}$) of the gas passing over the mirror depending on the physical state of the condensate (Wiederhold, 1997).

Particle backscatter and relative humidity

M. Brabec et al.

Title Page

Abstract

Introduction

Conclusions

References

Tables

Figures

◀

▶

◀

▶

Back

Close

Full Screen / Esc

Printer-friendly Version

Interactive Discussion



We calculate relative humidity with respect to ice according to its definition:

$$RH_{\text{ice}} = \frac{e_{\text{ice}}(T_{\text{mirror}})}{e_{\text{ice}}(T_{\text{ambient}})},$$

where $e_{\text{ice}}(T)$ is the saturation water vapour pressure over ice at temperature T . The functional dependence of the vapour pressure, $e_{\text{ice}}(T)$, is determined from the vapour pressure formula of Murphy and Koop (2005). The uncertainty of the frost point measurement, including an uncertainty of 0.2°C in the air temperature measurement, is approximately 0.5°C (Vömel et al., 2007). A conservative estimate of the overall uncertainty in the relative humidity covering our altitude range is 8% of the reported RH_{ice} value, i.e. $\Delta RH_{\text{ice}} = \pm 8\%$ at saturation and $\Delta RH_{\text{ice}} = \pm 10.4\%$ at the maximum saturation ratio corresponding to $RH_{\text{ice}} = 130\%$ observed on 6 November 2008 above Lindenberg.

2.3 Meteorological data

Fields of horizontal and vertical winds, pressures, temperatures, specific humidities and ice water contents from global operational analyses performed by the European Centre for Medium Range Weather Forecast (ECMWF) with roughly $1^\circ \times 1^\circ$ horizontal and 1 km upper tropospheric vertical resolution have been stored every 6 h and compared with the sonde measurements on 6 November 2008. The ECMWF data fail to represent the measured ice water contents and relative humidities. Insufficient spatial and temporal resolutions are likely reasons for this deficiency.

Therefore we have also compared with regional COSMO-7 from MeteoSwiss. COSMO-7 is based on the model COSMO of the “COntsortium for Small-scale MOdelling” (Doms et al., 2011). It is a non-hydrostatic limited-area model developed for operational and research applications on the meso-beta and meso-gamma scale (Stepheler et al., 2003). The model is based on thermo-hydrodynamical equations describing compressible flow in a moist atmosphere. The model equations are formulated in rotated geographical coordinates and a generalised terrain following height coordinate.

Particle backscatter and relative humidity

M. Brabec et al.

Title Page

Abstract

Introduction

Conclusions

References

Tables

Figures

◀

▶

◀

▶

Back

Close

Full Screen / Esc

Printer-friendly Version

Interactive Discussion



A variety of physical processes are taken into account by parameterization schemes (Doms et al., 2011). COSMO-7 has 6.6 km × 6.6 km horizontal and about 0.5 km vertical resolution in the upper troposphere. Instead of the characteristic hourly output we used high resolution output every 5 min (while the COSMO-7 internal time step is 60 s) from one forecast (6 November 2008, 18:00 UTC) covering the region of interest.

2.4 Trajectory calculation

Trajectories are calculated with the three dimensional LAGRangian ANalysis TOol (LAGRANTO), which is explained in detail by Wernli and Davies (1997). LAGRANTO is forced by meteorological input data, e.g. from COSMO-7 forecast wind fields. In LAGRANTO the forecast fields are interpolated linearly in space and time using the two nearest stored forecast fields. LAGRANTO has successfully been used in the past to investigate cirrus cloud processes (Colberg et al., 2003; Fueglistaler et al., 2004; Spichtinger et al., 2005b).

2.5 Microphysical/optical column model

We have employed our state-of-the-art microphysical box model (ZOMM) along COSMO-7-based LAGRANTO trajectories, in order to obtain the ice particle size distribution (dn/dr) in full detail. The model simulates homogeneous ice nucleation and growth/evaporation including vapour diffusion and surface mass accommodation (while particle number densities are sufficiently small to render coagulation processes unimportant). In a pure box model configuration this model has previously been utilized for polar stratospheric cloud simulations (Luo et al., 2003a). With stacked boxes the model has also been used as a column model, which allows approximating particle sedimentation (Luo et al., 2003b). The case investigated here is practically devoid of horizontal wind shear and is therefore well suited for a column approach. (Vertical wind shear may compromise the model results; however, the length-to-thickness aspect ratio

Particle backscatter and relative humidity

M. Brabec et al.

Title Page

Abstract

Introduction

Conclusions

References

Tables

Figures

◀

▶

◀

▶

Back

Close

Full Screen / Esc

Printer-friendly Version

Interactive Discussion



of the cirrus clouds is sufficiently large to suggest quasi-uniform conditions along the cloud for ice particles sedimenting from the upper to the lower cloud edge.)

The particle model is Lagrangian in radius space for the condensed phase, i.e. the model follows the freshly nucleated particles and creates a new size class (i) each time there is new ice particle nucleation. The model then transports the ice particles of class i downstream with time-dependent radius $r_i(t)$ and constant number density, n_i . The model treats the vapour phase in an Eulerian scheme, with air parcels driven by temperature and pressure data along LAGRANTO trajectories. Upstream of the cloud, the air parcels are stacked in equal vertical distances of 50 m in the vertical column (this distance may change slightly downstream due to inhomogeneities in the vertical air motions) between 6 and 14 km. Also sedimentation of ice particles is treated in this Eulerian space, allowing the particles to sediment within the stacked column, i.e. a fraction of n_i of class i is removed according to the size-dependent sedimentation speed v_i and reinjected to the box below. The sedimenting ice particles are then added to the preexisting two neighboring ice bins, when the mass of ice particles differ less than 20 %, otherwise, a new size ice bin is created.

The microphysical column model performs a fully kinetic treatment of the ice particle size distribution including a partitioning of water between the vapour and condensed phases. These calculations are based on a comprehensive homogeneous ice nucleation parameterization and a condensation/evaporation calculation by solving the diffusion equation (including mass accommodation on the ice surface), which allow a much more detailed physical treatment than the equilibrium bulk cloud schemes used by ECMWF or in COSMO-7. The Lagrangian size treatment avoids “numerical diffusion”, leading to artificial redistributions of particle number densities on a fixed Eulerian size grid. The initial aerosol particle distribution is chosen as lognormal with a mode radius $r_m = 0.06 \mu\text{m}$, a lognormal width $\sigma = 1.8$ and a total number density $n = 200 \text{cm}^{-3}$, reflecting typical upper tropospheric aerosol size distributions at midlatitudes. The computations are initialized at suitable trajectory points upstream, where the underlying NWP suggests the air to be cloud-free (this procedure avoids having to initialize ice

**Particle backscatter
and relative humidity**

M. Brabec et al.

Title Page

Abstract

Introduction

Conclusions

References

Tables

Figures

◀

▶

◀

▶

Back

Close

Full Screen / Esc

Printer-friendly Version

Interactive Discussion



**Particle backscatter
and relative humidity**

M. Brabec et al.

Title Page

Abstract

Introduction

Conclusions

References

Tables

Figures

◀

▶

◀

▶

Back

Close

Full Screen / Esc

Printer-friendly Version

Interactive Discussion



size distributions). Following Koop et al. (2000) homogeneous ice nucleation rates are calculated from saturation ratios (RH) and temperature (T) along each trajectory. Once formed, ice particles compete in uptake of water vapour from the gas phase at the expense of the liquid, diluted aerosol particles or, in a mixed phase cloud, the water cloud droplets, the so-called Bergeron-Findeisen effect (Seinfeld and Pandis, 1998). The ice growth eventually depletes the vapour phase and relaxes the ice supersaturation. In combination with the nucleation scheme the diffusion limited treatment yields realistic ice particle number densities (Hoyle et al., 2005) and size distributions depending on the cooling rates prescribed by the trajectories, with the possibility to superimpose small-scale temperature fluctuations, $(dT/dt)_{ss}$.

Finally, an optical module uses the particle size distributions calculated by means of the microphysical model in order to calculate the backscatter ratios measured by COBALD at 455 nm (blue) and 870 nm (infrared). To this end, the backscatter of spherical particles, such as aerosol droplets and cloud drops, are computed in an exact manner by solving the scattering problem by means of a Mie code. Aspherical particles, such as ice crystals, are approximated as prolate (“cigar-like”) spheroids with aspect ratio $A = a/b$ (the ratio of the equatorial to polar lengths) and volume $V = 4/3\pi a^2 b$, which is taken equal to the volume of the ice particles calculated by the microphysical model. Calculations were then made using a T-matrix light scattering algorithm (Mishchenko, 1991; Carslaw et al., 1998) with a refractive index of ice of 1.31 at 455 and 870 nm and assuming an aspect ratio $A = 0.75$, which is a typical value for midlatitude cirrus cloud particles (Nousiainen and McFarquhar, 2004).

3 Observations

On 6 November 2008 just after 00:00 UTC the COBALD-CFH tandem was launched on a radio sonde from Lindenberg as part of the LUAMI campaign. During this night North-Eastern Germany was covered by a 400-m thick inversion layer with thick radiation fog, which rendered the employment of ground-based Lidars impossible. In addition to the

optically thick radiation fog layer Fig. 1 shows two high-altitude cirrus clouds revealed by the COBALD and CFH measurements.

The upper tropospheric weather situation during this night is characterized by very little horizontal wind shear and wave-induced ice nucleation a few hours upstream, making it ideal for detailed testing of cirrus modelling. This is detailed in Figs. A1 and A2 of Appendix A.

The particle backscatter ratios (BSR) and relative humidities RH_{ice} in Fig. 1 unambiguously reveal the two layers of subvisible cirrus clouds. Each of these two cirrus layers has a geometric thickness of about 600 m and an optical thickness $\tau \leq 0.03$, i.e., they are “subvisible” according to the classification of Sassen (2002). The upper cirrus “U” has a clearly defined lower edge at 11 400 m and a less distinct upper edge. Inside and just below this cloud the gas phase is saturated with respect to ice (CFH measurements shown as cyan line), while a distinct layer extending from the upper cloud edge to roughly 500 m above the cloud reveals a supersaturation of up to $\sim 25\%$. The second cirrus layer “L” has its lower edge at 8300 m. Cloud “L” was reached at 00:36 UTC and cloud “U” at 00:44 UTC on 6 November 2008. Also cloud “L” shows a distinct layer with up to $\sim 30\%$ supersaturation just above it and partly overlapping with the cloud, while the lower end of the cloud is subsaturated by $\sim 50\%$ and obviously evaporating rapidly.

Without the COBALD measurements, i.e. based only on the CFH measurements, it would not be possible to determine the existence of a cloud, let alone the borders of the two cirrus clouds. For example, it would be impossible to reveal for cloud “L” that half of the supersaturated layer is within the cloud and the other half above it. This demonstrates that adding COBALD to the balloon payload is essential for localizing, and therefore analyzing cirrus properly.

The observed clear-sky supersaturations of 30 % are not surprising; for example homogeneous ice nucleation requires more than 45 % supersaturation under midlatitude upper tropospheric conditions (Koop et al., 2000). The range of $RH_{ice} = 50\% - 130\%$ inside the lower cirrus might be more surprising at first sight, but only detailed cloud

**Particle backscatter
and relative humidity**

M. Brabec et al.

Title Page

Abstract

Introduction

Conclusions

References

Tables

Figures

◀

▶

◀

▶

Back

Close

Full Screen / Esc

Printer-friendly Version

Interactive Discussion



modelling can help clarifying whether such non-equilibrium conditions are to be expected (see Sects. 5 and 6).

4 Analyzing COSMO-7 fields

We have compared the measurements in Fig. 1 with the 00:00 UTC ECMWF operational analysis data above Lindenberg, Germany on 6 November 2008. However, the ECMWF analysis fails to generate the observed clouds or humidities: the ice water content (IWC) is zero at any altitude at the time of the observation. The ECMWF analysis succeeds in obtaining realistic RH_{ice} in the vicinity of the upper cloud “U”, however, without triggering ice nucleation, and it completely misses the supersaturation close to the lower cloud “L”. Backward trajectories based on the 6-hourly analysis output reveal that the air parcel ending at “L” had developed a cirrus cloud at 12:00 UTC on 5 November (with $IWC = 0.018 \text{ g kg}^{-1}$), but this cloud led to a too rapid dehydration of this layer, and the ice disappeared completely from the entire air column by the time of the measurement.

Figure 2 shows direct comparisons of the measurements with the COSMO-7 forecast results. The black lines in all four panels of Fig. 2 represent COSMO-7 (00:35 and 00:45 UTC) forecast data above Lindenberg, Germany on 6 November 2008. The cyan lines in the upper two panels represent RH_{ice} measured by CFH and the horizontal grey bars show the locations of the cloud deduced from the backscatter measurements.

A difficulty arises when we want to compare the backscatter ratios (BSR) measured by COBALD with the COSMO-7 IWC, which is the only condensed phase quantity provided by the ice bulk scheme of the regional weather forecast model. The difficulty stems from the fact that the two BSR do not provide sufficient information to derive the complete size distribution, which would in principle be required for an exact derivation of the IWC. Clouds with the same BSR at a given wavelength can have different IWC if they have different particle sizes and number densities. However, as both the IWC and a BSR are integral measures of condensed water per volume of air, there is a robust

Particle backscatter and relative humidity

M. Brabec et al.

Title Page

Abstract

Introduction

Conclusions

References

Tables

Figures

◀

▶

◀

▶

Back

Close

Full Screen / Esc

Printer-friendly Version

Interactive Discussion



relationship between the two, and only a weaker dependence on the details of the size distribution. Appendix B shows that a measurement of BSR at 870 nm within a thin high cirrus cloud constrains its IWC to within a factor of ~ 4 . The blue points in the lower two panels of Fig. 2 show the estimation of the maximum IWC within the clouds based on the maximum BSR at 870 nm measured by COBALD, and the horizontal error bars show the uncertainties described above.

RH_{ice} from COSMO-7 data at 00:35 and 00:45 UTC in Fig. 2, while unable to provide the fine filamentary structure captured by CFH, shows general features in agreement with the CFH measurement. In particular, COSMO-7 correctly represents the characteristic double hump in RH_{ice} with two layers of saturation or slight supersaturation; this is the basis for the development of two distinct cirrus layers. However, the modeled supersaturations do not reach the high values shown by CFH, probably because the lack of a kinetic treatment of ice particle growth empties the vapour phase too quickly. Furthermore, the modeled RH_{ice} profile appears to be shifted downward in comparison to the measurement, suggesting that the ice particles modeled by COSMO-7 might grow to too large sizes and therefore might sediment too rapidly.

The IWC of the COSMO-7 fields in the lower panels of Fig. 2 clearly display two cirrus clouds in agreement with COBALD. However, the upper cloud “U” resides at a too low an altitude and the IWC is much too small. The underestimation of IWC is at least a factor of 2, more likely a factor of 5 (taking the uncertainties in the derivation of IWC from the COBALD data into account).

5 Trajectory-based microphysical analysis without small-scale $(dT/dt)_{ss}$

As described in Sects. 2.4 and 2.5 we have used the microphysical column model, driven along LAGRANTO backward trajectories directly based on COSMO-7 forecast fields, i.e. *without* consideration of unresolved small-scale temperature fluctuations, $(dT/dt)_{ss}$. Panel (a) in Fig. 3 shows BSR at 870 nm during the last 8 h of these trajectories before arriving above Lindenberg (at $t = 0$). The lower cloud “L” forms at -6 h

Particle backscatter and relative humidity

M. Brabec et al.

[Title Page](#)[Abstract](#)[Introduction](#)[Conclusions](#)[References](#)[Tables](#)[Figures](#)[◀](#)[▶](#)[◀](#)[▶](#)[Back](#)[Close](#)[Full Screen / Esc](#)[Printer-friendly Version](#)[Interactive Discussion](#)

**Particle backscatter
and relative humidity**

M. Brabec et al.

Title Page

Abstract

Introduction

Conclusions

References

Tables

Figures

◀

▶

◀

▶

Back

Close

Full Screen / Esc

Printer-friendly Version

Interactive Discussion



through homogenous nucleation above the Upper Tauern mountain chain (see Appendix A). In the first few hours of lifetime of “L” the BSR reaches values of more than 500, indicating an optically thick cirrus cloud. This is in accordance with the satellite images (Fig. A1 at $t = -5$ h). At around $t = -0.7$ h the cloud has almost fully evaporated, leaving only a small remainder in the modeled BSR profile (black line in panel (b) of Fig. 3), with an aerosol backscatter ratio $ABSR = BSR - 1$ about 5-times smaller than measured by COBALD (red line).

The upper cloud “U” starts to form only at $t = -1.5$ h, related to a slow upwelling of the air above the East German flatlands. However, the ice crystals sediment much too rapidly, and cloud “U” evaporates fully at $t = -0.6$ h. The high sedimentation rates are suggestive of too few, too large ice crystals that form in the microphysical column model along the COSMO-7-derived in the absence of $(dT/dt)_{ss}$. As a consequence, the model fails to reproduce the upper cloud.

6 Trajectory-based microphysical analysis including small-scale $(dT/dt)_{ss}$

The results shown in Sect. 5 indicate that in order to reproduce the observed clouds it appears to be necessary to superimpose small-scale temperature fluctuations, $(dT/dt)_{ss}$, that remain unresolved by the mesoscale trajectories, as has also been suggested by Hoyle et al. (2005). In the following we will use $(dT/dt)_{ss}$ based on measurements from the “Subsonic Aircraft: Contrail and Cloud Effects Special Study” (SUCCESS). The procedure is similar to that employed by Hoyle et al. (2005). However, while these authors have superimposed $(dT/dt)_{ss}$ directly from the SUCCESS vertical wind measurements onto ERA-40 trajectories with a resolution of roughly $275\text{ km} \times 275\text{ km}$ and meteorological input fields of every 6 h (or, for simplicity and without loss of accuracy, on a trajectory with a small constant cooling rate), we need to take into account that our COSMO-7 fields with $6.6\text{ km} \times 6.6\text{ km}$ every 5 min (see Appendix C) have a much better resolution, so that the larger scale fluctuations will already be included. Therefore, we performed a Fourier analysis of the SUCCESS data and kept

only contributions to $(dT/dt)_{ss}$ corresponding to wavelengths smaller than 30 km, as contributions with longer wavelengths will likely be fully resolved on the 6.6-km grid of COSMO-7 (assuming that 4 grid points are required to resolve a small-scale feature). The remaining $(dT/dt)_{ss}$ are applied with peak-to-peak amplitudes of 1 K with random frequencies. Figure 4 shows one example, where the solid line represents the temperature along one COSMO-7-based LAGRANTO trajectory with the superimposed small-scale fluctuations shown as dotted line.

Figure 5 shows results obtained from the microphysical column model driven along COSMO-7-based LAGRANTO trajectories with superimposed small-scale temperature fluctuations (see in addition Fig. B2). The left side of the figure shows BSR and how the ice crystals persist until the time of the measurement (panel a). This modelling approach develops two cloud layers and is overall a much more accurate description of the measurements than the result without $(dT/dt)_{ss}$ shown in Fig. 3. However, specific discrepancies remain. The modeled lower cloud “L” is only half as thick as observed, but the BSR intensity is about 4 times larger at its peak (Fig. 5b). The modeled upper cloud “U” resides at an altitude about 1 km too low, but agrees well in intensity with the measurement.

The right side of Fig. 5 shows RH_{ice} , which does not differ much from the results in Fig. 3. Panel (c) displays the evolution of RH_{ice} during the 8 h before the measurement. Panel (d) shows that the general features of the modeled and measured RH_{ice} profiles agree well, but the modeled values are somewhat too low in the vicinity of the upper cloud “U”. The in-cloud measurements showed that RH_{ice} varied between 50 % and 130 %. For both clouds profiles of RH_{ice} and BSR are vertically displaced, i.e. the BSR maxima are located below the RH_{ice} maxima (or actually sit close to the transition point of super- to subsaturation), which is likely due to particle sedimentation. The modeled in-cloud RH_{ice} covers only the range from 80 % to 105 %, i.e. in the model sub- and supersaturations tend to relax too rapidly. This suggests a delicate interplay between RH_{ice} and $(dT/dt)_{ss}$: in the absence of $(dT/dt)_{ss}$ ice number densities are small, particle grow to large sizes, sediment rapidly and allow for large deviations from

**Particle backscatter
and relative humidity**

M. Brabec et al.

[Title Page](#)[Abstract](#)[Introduction](#)[Conclusions](#)[References](#)[Tables](#)[Figures](#)[◀](#)[▶](#)[◀](#)[▶](#)[Back](#)[Close](#)[Full Screen / Esc](#)[Printer-friendly Version](#)[Interactive Discussion](#)

saturation; conversely, with $(dT/dt)_{ss}$ ice number densities are generally larger, particle stay smaller, sediment less rapidly and lead to faster equilibrations of in-cloud sub- and supersaturations. Improved agreement between model and measurement might be achieved if the mass accommodation coefficient of the H_2O molecules on the ice surface was assumed to be much smaller than unity (the value used in the present calculations) or was dependent on the degree of supersaturation.

In order to test the dependence of the modeled cirrus on the superimposed $(dT/dt)_{ss}$ we performed an ensemble calculation with 20 runs using the microphysical column model and applying the temperature fluctuations obtained by random superpositions of different frequencies. The results are displayed in Fig. 6 as blue lines, while the measurements are shown as red line. In general the 20 runs are very similar: 18 of the 20 runs produce two fully developed cloud layers, while 2 runs show only a marginal upper cloud (left panel), and RH_{ice} displays only small differences between the 20 runs (right panel). However, the left panel shows also that the position and width of the lower cloud vary in dependence on the way the temperature fluctuations are superimposed. The upper cloud is in all 20 cases too low in altitude, which is an error likely due to the COSMO-7 cloud scheme dehydrating the air too strongly in an upstream cloud event. Within all ensemble calculations in-cloud RH_{ice} cover the range from 70 % to 130 %. This is in better agreement with the observed variation between 50 % and 130 %, at least concerning the supersaturation. The still too small subsaturation might be an indication that the ice particles, after applying $(dT/dt)_{ss}$, are slightly too small and do not sediment sufficiently quickly into even dryer layers of air.

Finally, we analyzed the profiles at slightly displaced geographical positions. The evolution of BSR in Fig. 5 suggests that both clouds underwent evaporation during the measurement. Therefore we checked whether COSMO-7 simply displaced the profiles and captured the situation shifted by 30 km to the north, east, south or west of Lindenberg. This analysis (not shown here) reveals that the upper cloud varies somewhat in altitude (by less than 1 km) depending on the geographical position. This is an indication for waves in this region, as is also depicted in Fig. A2. Indeed, the model provides

**Particle backscatter
and relative humidity**

M. Brabec et al.

Title Page

Abstract

Introduction

Conclusions

References

Tables

Figures

◀

▶

◀

▶

Back

Close

Full Screen / Esc

Printer-friendly Version

Interactive Discussion



better agreement with the measurements when evaluated at 30 km south of Lindenberg (i.e. upstream), whereas the balloon drifted northward.

7 Summary and conclusion

This work has analyzed balloon-borne sonde measurements of two cirrus layers above Lindenberg, Germany on 6 November 2008. The newly developed backscatter sonde COBALD and the state-of-the-art frost point hygrometer CFH were used as part of the “Lindenberg Upper-Air Methods Intercomparison” (LUAMI) campaign. The COBALD-CFH tandem is shown to be an excellent combination to determine the partitioning of atmospheric water between the gas phase and the condensed ice phase in and around cirrus clouds, and thus to detect in-cloud and out-of-cloud supersaturation with respect to ice. In-cloud measurements showed that RH_{ice} varied from 50 % to 130 %, with supersaturations occurring at the cloud upper edges, and subsaturation at the cloud lower edges, reflecting the regions of fresh nucleation and particle evaporation in fall streaks, respectively.

In contrast to the too coarsely resolved ECMWF analysis data, COSMO-7 forecast fields (6.6 km \times 6.6 km, 5 min resolution, Appendix C) enable to obtain good agreement with the observations, though the cloud altitude and thus the profile of the ice water content is not captured accurately. Also, COSMO-7 shows generally smaller in-cloud or out-of-cloud supersaturations than were observed by CFH. Comprehensive micro-physical cloud model calculations along LAGRANTO trajectories based on COSMO-7 wind and temperature fields allow humidity, ice particle size, number density and backscatter ratios to be determined much more accurately than the COSMO-7 cloud scheme. However, satisfying agreement with the measurements can only be obtained after superimposing small-scale temperature fluctuations, $(dT/dt)_{ss}$, onto the COSMO-7-based trajectories. In an ensemble model-calculation of 20 runs with randomly superimposed small-scale temperature fluctuations $(dT/dt)_{ss}$ in-cloud supersaturations of up to 30 % are reached, which is in agreement with the measurements. Therefore, the

Particle backscatter and relative humidity

M. Brabec et al.

Title Page

Abstract

Introduction

Conclusions

References

Tables

Figures

◀

▶

◀

▶

Back

Close

Full Screen / Esc

Printer-friendly Version

Interactive Discussion



present study, although providing observational evidence for high in-cloud supersaturation, does not call for new physical mechanisms required to explain the apparent supersaturation.

Appendix A

5 Upper tropospheric weather on 6 November 2008

Figure A1 shows cloud images from the Meteosat-9 satellite at four different times during the night of 5–6 November 2008. The selected channel is the Thermal Infrared, IR 10.8 μm . The gray scale visualises temperatures. Bright regions indicate cold clouds, e.g. convective systems or outflows thereof. Conversely, very dark regions indicate clear sky. Grey tones indicate low-level clouds or fog. Fine differences in grey shading over Northeastern Germany and Western Poland suggest banks of low-level clouds or fog, such as the 400-m thick radiative fog layer prevailing in Lindenberg during this night. In contrast, the subvisible cirrus clouds measured by COBALD around 8.5 and 11.9 km remain undetectable for Meteosat. The white lines superimposed on the Meteosat images are projections of the two COSMO-7-based LAGRANTO trajectories ending in the upper and lower subvisible cirrus, “U” and “L”, at 00:35 and 00:45 UTC, respectively. The white circles indicate the respective positions of air parcels at -7h , -5h and -3h upstream, eventually arriving at “U” and “L” over Lindenberg. The absence of bright features in the vicinity of the air parcel positions suggests that the air has not been directly affected by convective outflow, rather has been subject to wave-driven cooling when the air is driven across the main chain of the Alps. The similar development of the two trajectories shows the absence of horizontal wind shear.

Figure A2 shows an altitude-resolved array of COSMO-7-based LAGRANTO backward trajectories ending at the balloon flight path at time $t = 0$ around 52.2°N . The two trajectories marked in red and green depict the air parcel paths ending in the lower cloud “L” and upper cloud “U”, respectively. The left panel of Fig. A2 shows the gravity

Particle backscatter and relative humidity

M. Brabec et al.

Title Page

Abstract

Introduction

Conclusions

References

Tables

Figures

◀

▶

◀

▶

Back

Close

Full Screen / Esc

Printer-friendly Version

Interactive Discussion



waves being assembled at different times, due to some vertical wind shear. The right panel shows the same trajectories but plotted as pressure vs. latitude, revealing the waves to be generated around 47° N at almost all altitudes.

These waves are caused by the main chain of the Alps. The maximum wave activity is located around 47° N–13° E, the region of the Upper Tauern, a West-East oriented mountain chain in Austria, which reaches up to 3800 m altitude. The absence of horizontal wind shear and the wind direction being almost orthogonal to the mountain ridge are ideal prerequisites for the development of the mountain-wave induced cirrus clouds.

Appendix B

Estimation of the IWC from the measured ABSR

Obtaining an estimate of the IWC from the aerosol backscatter ratio ABSR measured by COBALD is not possible in an exact manner, because the size distribution is generally not known. However, if the distribution can be approximated as lognormal with constant width σ and if rough estimates of the mode radius r_m exist, an approximate IWC-ABSR relationship is readily obtained, including an error estimate. Figure B1 shows simulated ABSR at wavelength 870 nm for $IWC = 10^{-3} \text{ g kg}^{-1}$ condensed as ice in a lognormal size distribution as function of r_m . The assumed lognormal size distribution width is $\sigma = 1.4$, the refractive index is that of ice (1.31), and the aspect ratio of the aspherical particles is $A = 0.75$.

An ice water content of $10^{-3} \text{ g kg}^{-1}$ corresponds to only 1.6 ppmv H_2O in the condensed ice phase, i.e. a very thin subvisible cloud. This calculation is easily applied to higher condensed masses by multiplying the ordinate with the appropriate IWC. The calculation reveals a significant, but overall weak dependence on the mode radius r_m . Typical values for r_m depend on the altitude and production process of the cirrus cloud. While cirrus decks from deep convective outflow may contain very large ice particles

Particle backscatter and relative humidity

M. Brabec et al.

Title Page

Abstract

Introduction

Conclusions

References

Tables

Figures

◀

▶

◀

▶

Back

Close

Full Screen / Esc

Printer-friendly Version

Interactive Discussion



with radii larger than 100 μm , the clouds of interest here contain ice crystals with typical radii between 5 μm and 20 μm . See for example the results from the microphysical box model calculations in Fig. B2, which belong to the model run shown in Fig. 5 and detailed in Sect. 6. The resulting range of ABSR corresponds to an overall uncertainty of a factor ~ 4 (dashed lines in Fig. B1).

Applying these considerations to the COBALD measurements in clouds “L” and “U” yields the blue points and error bars for IWC in the lower panels of Fig. 2.

Appendix C

5-min stored fields of COSMO-7

A special research data set was assembled storing COSMO-7 fields every 5 min instead of the usual hourly storage. This was done after it had become clear that the quality of the microphysical model will depend crucially on capturing the correct cooling rates, i.e. small-scale temperature fluctuations, $(dT/dt)_{SS}$. We used this opportunity to examine whether the high spatial or the high temporal resolution is more important for providing the meteorological conditions required for the ice cloud microphysics. Figure C1 shows for both the upper (“U”) and lower (“L”) cloud the LAGRANTO-derived backward trajectories, either based on the 5-min wind fields as input and 5-min trajectory output (black lines) or based on hourly wind fields, which are simply a subset of the 5-min dataset (bluish lines). The 1-h-based trajectory data show either also the interpolated data (dark blue) or only the 1-h data (cyan). The interpolated data (dark blue) provide cooling and heating rates which are comparable to the 5-min based dataset, much better than the trajectory data that provide only the hourly trajectory data. This suggests that interpolating trajectory data is actually a microphysically sensible procedure, even though the interpolation is of course not fully accurate. The reason for this benign behavior is that trajectories pick up the high spatial resolution of COSMO-7 (6.6 km \times 6.6 km), including orography and weather systems, even when the temporal

Particle backscatter and relative humidity

M. Brabec et al.

Title Page

Abstract

Introduction

Conclusions

References

Tables

Figures

◀

▶

◀

▶

Back

Close

Full Screen / Esc

Printer-friendly Version

Interactive Discussion



storage is only hourly. Horizontal winds chase the air parcels much faster across this texture than the texture changes itself as function of time, at least in the cases examined here.

Acknowledgements. M. Brabec has been funded by the Swiss National Science Foundation under project number 200021-1179879. We also acknowledge ETH, Zurich, for financial support. Thanks to the organizers of the “Lindenberg Upper-Air Methods Intercomparison” campaign (LUAMI) and the whole crew in Lindenberg for excellent campaign work. We thank the European Centre for Medium Range Weather Forecast for the use of ECMWF analysis data. We gratefully acknowledge Petra Baumann from MeteoSwiss for the computation of the COSMO-7 weather forecasts performed at the Swiss National Supercomputing Centre (CSCS) in Manno, Switzerland. For LAGRANTO support we would like to acknowledge Michael Sprenger from ETH. We also gratefully acknowledge EUMETSAT for the satellite images.



This publication is supported by COST – www.cost.eu

References

- Beyerle, G., Gross, M., Haner, D., Kjome, N., McDermid, I., McGee, T., Rosen, J., Schäfer, H.-J., and Schrems, O.: A lidar and backscatter sonde measurement campaign at table mountain during february-march 1997: observations of cirrus clouds, *Am. Meteor. Soc.*, 15, 1275–1287, 2001.
- Carslaw, K. S., Wirth, M., Tsias, A., Luo, B. P., Dörnbrack, A., Leutbecher, M., Volkert, H., Renger, W., Bacmeister, J. T., and Peter, T.: Particle microphysics and chemistry in remotely observed mountain polar stratospheric clouds, *J. Geophys. Res.*, 103, 5785–5796, 1998.
- Christensen, J. H., Hewitson, B., Busuioc, A., Chen, A., Gao, X., Held, I., Jones, R., Kolli, R. K., Kwon, W.-T., Laprise, R., Magaña Rueda, V., Mearns, L., Menéndez, C. G., Räisänen, J., Rinke, A., Sarr, A., and Whetton, P.: Regional climate projections, in: *Climate Change 2007: The Physical Science Basis. Contribution of Working Group I to the Fourth Assessment Report of the Intergovernmental Panel on Climate Change*, edited by: Solomon, S., Qin, D., Manning, M., Chen, Z., Marquis, M., Averyt, K. B., Tignor, M., and Miller, H. L., Cambridge University Press, Cambridge, New York, 2007.

Particle backscatter and relative humidity

M. Brabec et al.

Title Page

Abstract

Introduction

Conclusions

References

Tables

Figures

◀

▶

◀

▶

Back

Close

Full Screen / Esc

Printer-friendly Version

Interactive Discussion



Colberg, C. A., Luo, B. P., Wernli, H., Koop, T., and Peter, Th.: A novel model to predict the physical state of atmospheric $\text{H}_2\text{SO}_4/\text{NH}_3/\text{H}_2\text{O}$ aerosol particles, *Atmos. Chem. Phys.*, 3, 909–924, doi:10.5194/acp-3-909-2003, 2003.

Doms, G., Förstner, J., Heise, E., Herzog, H.-J., Mironov, D., Raschendorfer, M., Reinhardt, T., Ritter, B., Schrodin, R., Schulz, J.-P., and Vogel, G.: A description of the nonhydrostatic regional COSMO model, Part II: physical parameterization, Deutscher Wetterdienst, P. O. Box 100465, 63004 Offenbach, Germany, available online at: <http://www.cosmo-model.org>, accessed on 27 December 2011.

EUMETSAT: Monitoring weather and climate from space, available online at: www.eumetsat.int, 2008.

Fueglistaler, S., Wernli, H., and Peter, T.: Tropical troposphere-to-stratosphere transport inferred from trajectory calculations, *J. Geophys. Res.*, 109, D03108, doi:10.1029/2003JD004069, 2004.

Hoyle, C., Luo, B., and Peter, T.: The origin of high ice crystal number densities in cirrus clouds, *J. Atmos. Sci.*, 62, 2586–2579, 2005.

Joos, H., Spichtinger, P., Lohmann, U., Gayet, J.-F., and Minikin, A.: Orographic cirrus in the global climate model ECHAM5, *J. Geophys. Res.*, 113, D18205, doi:10.1029/2007JD009605, 2008.

Koop, T., Luo, B., Tsias, A., and Peter, T.: Water activity as the determinant for homogeneous ice nucleation in aqueous solutions, *Nature*, 406, 611–614, 2000.

Larsen, N., Knudsen, B., Jorgensen, T. S., di Sarra, A., Fuà, D., Di Girolamo, P., Fiocco, G., Cacciani, M., Rosen, J., and Kjome, N.: Backscatter measurements of stratospheric aerosols at Thule during January–February 1992, *Geophys. Res. Lett.*, 21, 1303–1306, 1994.

Luo, B. P., Peter, T., Fueglistaler, S., Wernli, H., Wirth, M., Kiemele, C., Flentje, H., Yushkov, V. A., Khattatov, V., Rudakov, V., Thomas, A., Borrmann, S., Toci, G., Mazzinghi, P., Beuermann, J., Schiller, C., Cairo, F., Di Donfrancesco, G., Adriani, A., Volk, C. M., Strom, J., Noone, K., Mitev, V., MacKenzie, R. A., Carslaw, K. S., Trautmann, T., Santacesaria, V., and Stefanutti, L.: Dehydration potential of ultrathin clouds at the tropical tropopause, *Geophys. Res. Lett.*, 30, 1557, doi:10.1029/2002GL016737, 2003a.

Luo, B. P., Voigt, C., Fueglistaler, S., and Peter, T.: Extreme NAT supersaturations in mountain wave ice PSCs: a clue to NAT formation, *J. Geophys. Res.*, 108, 4441, doi:10.1029/2002JD003104, 2003b.

**Particle backscatter
and relative humidity**

M. Brabec et al.

Title Page

Abstract

Introduction

Conclusions

References

Tables

Figures

◀

▶

◀

▶

Back

Close

Full Screen / Esc

Printer-friendly Version

Interactive Discussion



Particle backscatter and relative humidity

M. Brabec et al.

Title Page

Abstract

Introduction

Conclusions

References

Tables

Figures

◀

▶

◀

▶

Back

Close

Full Screen / Esc

Printer-friendly Version

Interactive Discussion



MeteoSwiss: The numerical weather prediction model COSMO, website available under <http://www.meteoswiss.admin.ch/web/en/weather/models/cosmo.html>, last access: 30 January 2012.

Mishchenko, M. I.: Light scattering by randomly oriented axially symmetric particles, *J. Opt. Soc. Am.*, 8, 871–882, 1991.

Möhler, O., Fahey, D., and Gao, R.: Summary of the aquavit water vapor intercomparison: static experiments, website available under https://aquavit.icg.kfa-juelich.de/WhitePaper/AquaVITWhitePaper_Final_23Oct2009_6MB.pdf, last access: 16 March 2011.

Nash, J., Oakley T., Vömel H., and Wei, L. I.: WMO Intercomparison of high quality radiosonde systems, Instruments and observing methods, Report No. 107, available online at: http://www.wmo.int/pages/prog/www/IMOP/publications/IOM-107_Yangjiang.pdf, 2011.

Nousiainen, T. and McFarquhar, G. M.: Light scattering by quasi-spherical ice crystals, *J. Atmos. Sci.*, 61, 2229–2248, doi:10.1175/1520-0469(2004)061;2229:LSBQIC;2.0.CO;2, 2004.

Peter, T., Marcolli, C., Spichtinger, P., Corti, T., Baker, M. B., and Koop, T.: When dry air is too humid, *Science*, 314, 1399–1402, 2006.

Rosen, J. and Kjöme, N.: Backscattersonde: a new instrument for atmospheric aerosol research, *Appl. Opt.*, 30, 1552–1561, 1991.

Rosen, J., Kjöme, N., and Liley, B.: Tropospheric aerosol backscatter at a midlatitude site in the Northern and Southern Hemispheres, *J. Geophys. Res.*, 102, 21329–21339, 1997.

Sassen, K.: Cirrus clouds, in: *Cirrus*, edited by: Lynch, D. K., Sassen, K., Starr, D. O. and Stephens, G., Oxford University Press, 11–40, 2002

Seinfeld, J. and Pandis, S.: *Atmospheric Chemistry and Physics: from Air Pollution to Climate Change*, Wiley-Interscience, New York, 1326 pp., 1998.

Spichtinger, P., Gierens, K., and Dörnbrack, A.: Formation of ice supersaturation by mesoscale gravity waves, *Atmos. Chem. Phys.*, 5, 1243–1255, doi:10.5194/acp-5-1243-2005, 2005a.

Spichtinger, P., Gierens, K., and Wernli, H.: A case study on the formation and evolution of ice supersaturation in the vicinity of a warm conveyor belt's outflow region, *Atmos. Chem. Phys.*, 5, 973–987, doi:10.5194/acp-5-973-2005, 2005b.

Stappeler, J., Doms, G., Schättler, U., Bitzer, H. W., Gassmann, A., Damrath, U., and Gregoric, G.: Meso-gamma scale forecasts using the nonhydrostatic model LM, *Meteorol. Atmos. Phys.*, 82, 75–96, 2003.

Toon, O. B. and Miake-Lye, R. C.: Subsonic aircraft: Contrail and Cloud Effects Special Study (SUCCESS), *Geophys. Res. Lett.*, 25, 1109–1112, 1998.

Vömel, H., David, D., and Smith, K.: Accuracy of tropospheric and stratospheric water vapor measurements by cryogenic frost point hygrometer: Instrumental details and observations, *J. Geophys. Res.*, 112, D08305, doi:10.1029/2006JD007224, 2007.

Wernli, H. and Davies, H.: A lagrangian-based analysis of extratropical cyclones. I: The method and some applications, *Q. J. Roy. Meteorol. Soc.*, 123, 467–489, 1997.

Wiederhold, P.: *Water Vapor Measurement: Methods and Instrumentation*, Marcel Dekker, Inc., 353 pp., 1997.

Wienhold, F. G.: COBALD (Compact Optical Backscatter Aerosol Detector) Data Sheet, available online at: http://www.iac.ethz.ch/groups/peter/research/Balloon_soundings/COBALD_data_sheet, last access: 26 December 2011.

ACPD

12, 9553–9586, 2012

Particle backscatter and relative humidity

M. Brabec et al.

Title Page

Abstract

Introduction

Conclusions

References

Tables

Figures

◀

▶

◀

▶

Back

Close

Full Screen / Esc

Printer-friendly Version

Interactive Discussion



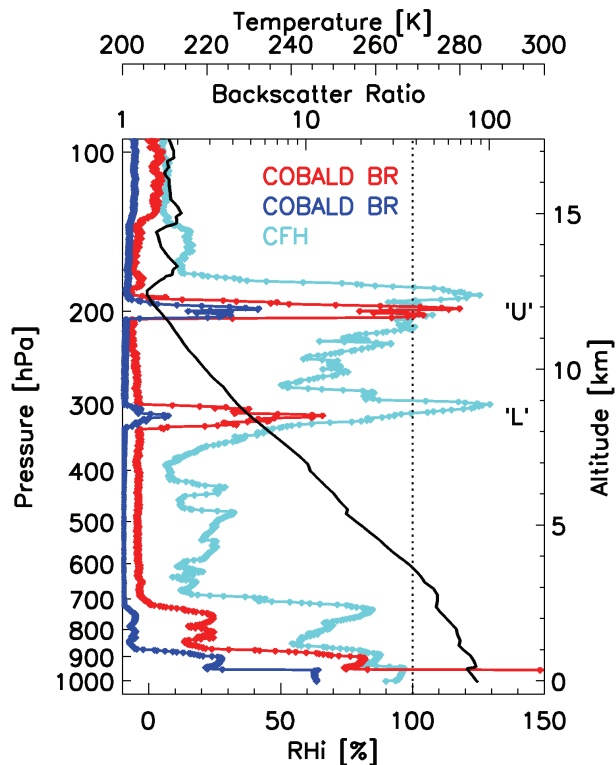


Fig. 1. Profile of balloon sounding on 6 November 2008 above Lindenberg, Germany. Blue and red lines: backscatter ratios (BSR) at 455 nm and 870 nm wavelength, respectively, measured by COBALD. Cyan line: relative humidity with respect to ice (RH_{ice}) obtained from the CFH frost point measurement. Quantities shown as function of barometric pressure and GPS-measured geometric altitude. The upper and lower cirrus clouds are termed “U” and “L”, respectively.

Particle backscatter and relative humidity

M. Brabec et al.

Discussion Paper | Discussion Paper | Discussion Paper | Discussion Paper | Discussion Paper

Title Page

Abstract Introduction

Conclusions References

Tables Figures

◀ ▶

◀ ▶

Back Close

Full Screen / Esc

Printer-friendly Version

Interactive Discussion



Particle backscatter
and relative humidity

M. Brabec et al.

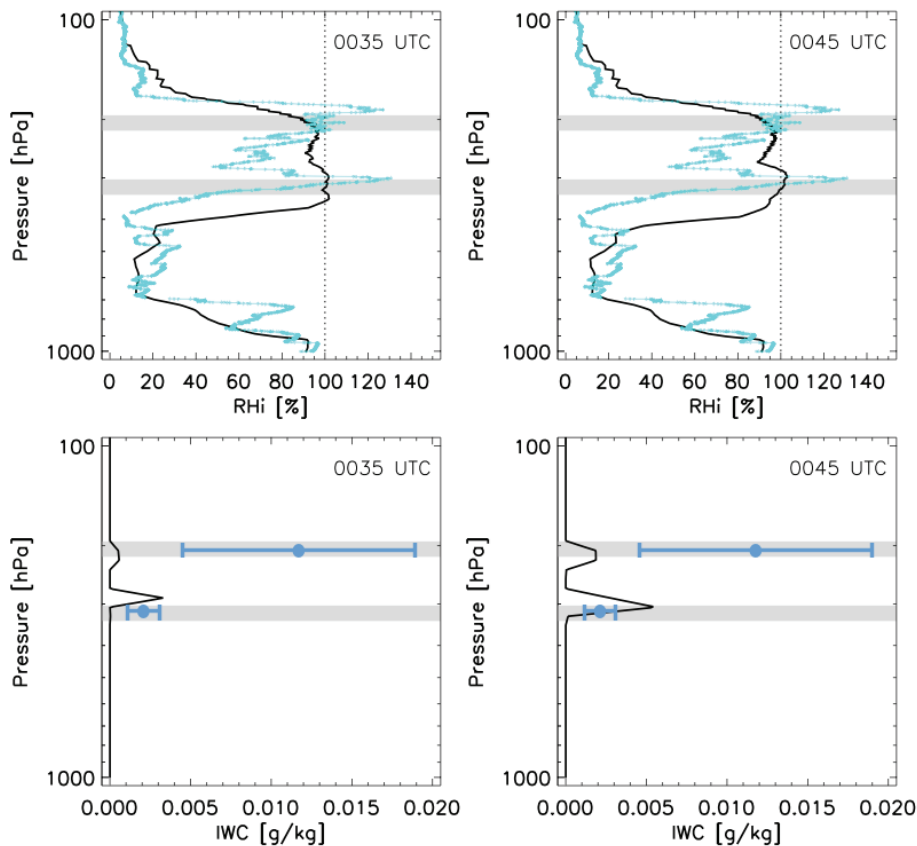


Fig. 2. RH_{ice} and IWC profiles of COSMO-7 forecast data (black lines) above Lindenberg on 6 November 2008. Left: sounding of lower cloud at 00:35 UTC. Right: sounding of upper cloud at 00:45 UTC. Cyan line: RH_{ice} profile measured by CFH. Grey horizontal bars: altitude ranges of the detected clouds. Blue bars in the lower two panels: IWC estimated from COBALD data as explained in Appendix A.

Particle backscatter
and relative humidity

M. Brabec et al.

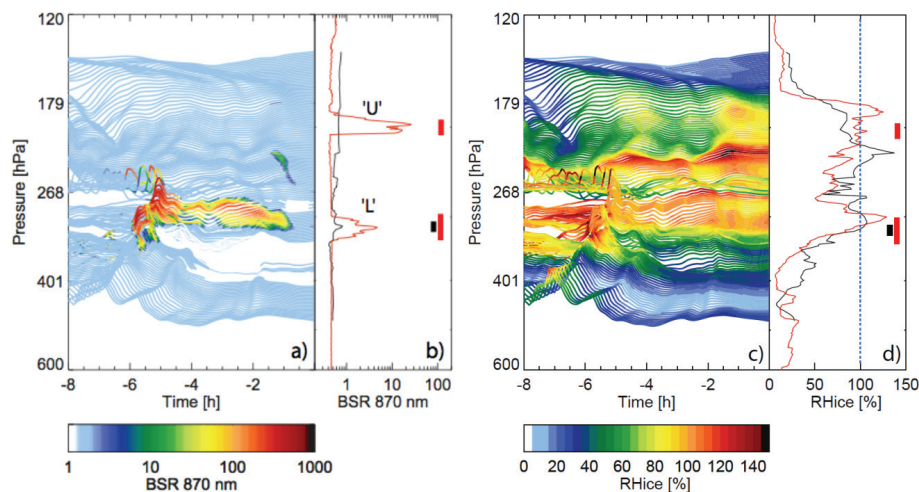


Fig. 3. Results from microphysical column model driven by plain COSMO-7-based LAGRANTO trajectories compared to measurements of backscatter ratio (BSR) at 870 nm wavelength (**a, b**) and relative humidity (RH_{ice}) with respect to ice (**c, d**). (**a, c**) Color-coded: modeled BSR and RH_{ice} . (**b, d**) Red curves: BSR and RH_{ice} profiles measured by COBALD and CFH, respectively; black curves: model results at $t = 0$ above Lindenberg (right edge of panels (**a**) and (**c**)). The model produces both clouds (“U” and “L”) a few hours upstream of the measurement, but due to too rapid sedimentation fails to maintain them until the measurement time. Red and black bars in panels (**b**) and (**d**) indicate the altitude ranges of the measured clouds and modeled cloud remnants, respectively.

Title Page

Abstract

Introduction

Conclusions

References

Tables

Figures

◀

▶

◀

▶

Back

Close

Full Screen / Esc

Printer-friendly Version

Interactive Discussion



Particle backscatter
and relative humidity

M. Brabec et al.

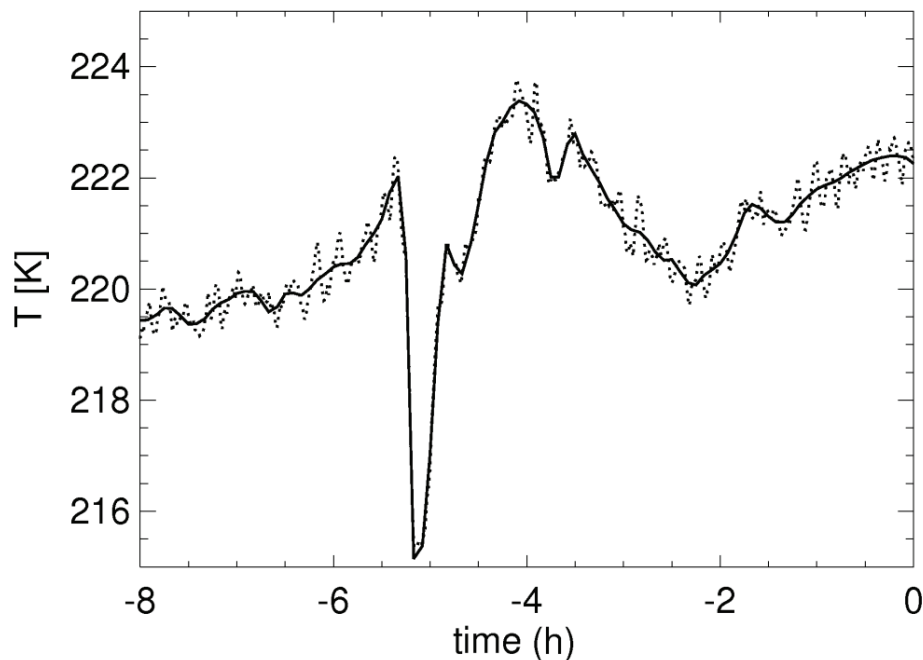


Fig. 4. Solid black line: temperature along a COSMO-7-based LAGRANTO trajectory in about 9 km altitude (close to cloud “L”). Dotted line: same trajectory with superimposed small-scale temperature fluctuations $(dT/dt)_{ss}$ (random superposition). The cooling rate spectrum has been determined from the peak-to-peak amplitude (1 K) and frequencies of $(dT/dt)_{ss}$ with wavelengths smaller than 30 km (see text) in agreement with the vertical wind measurements made during the SUCCESS campaign (see Hoyle et al., 2005).

[Title Page](#)[Abstract](#)[Introduction](#)[Conclusions](#)[References](#)[Tables](#)[Figures](#)[◀](#)[▶](#)[◀](#)[▶](#)[Back](#)[Close](#)[Full Screen / Esc](#)[Printer-friendly Version](#)[Interactive Discussion](#)

Particle backscatter
and relative humidity

M. Brabec et al.

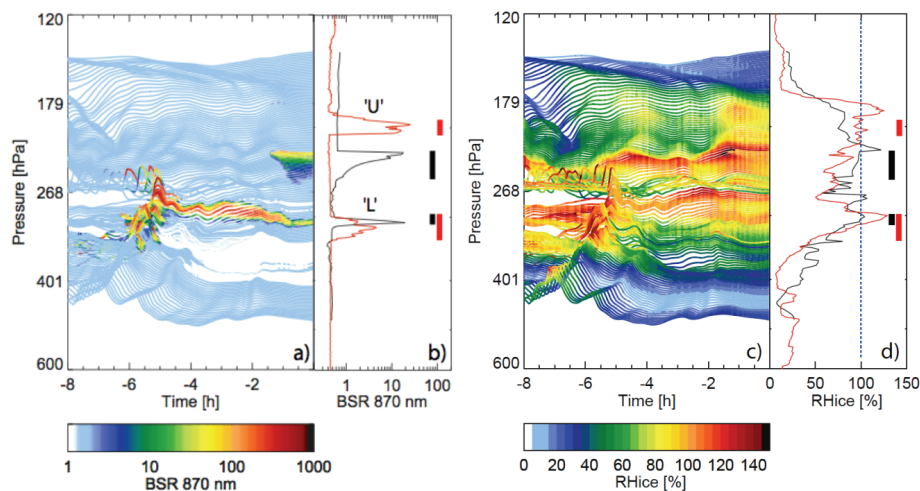


Fig. 5. Results from microphysical column model driven by COSMO-7-based LAGRANTO trajectories with superimposed small-scale temperature fluctuations (dT/dt)_{ss} compared to measurements of backscatter ratio (BSR) at 870 nm wavelength (**a, b**) and relative humidity (RH_{ice}) with respect to ice (**c, d**). (**a, c**) Color-coded: modeled BSR and RH_{ice}. (**b, d**) Red curves: BSR and RH_{ice} profiles measured by COBALD and CFH, respectively; black curves: model results at $t = 0$ above Lindenberg (right edge of panels (**a**) and (**c**)). The model produces both clouds (“U” and “L”) a few hours upstream of the measurement, and due to (dT/dt)_{ss} forms sufficiently small ice particles, which survive until the measurement time. Red and black bars in panels (**b**) and (**d**) indicate the altitude ranges of the measured and modeled clouds, respectively.

Title Page

Abstract

Introduction

Conclusions

References

Tables

Figures

◀

▶

◀

▶

Back

Close

Full Screen / Esc

Printer-friendly Version

Interactive Discussion



Particle backscatter
and relative humidity

M. Brabec et al.

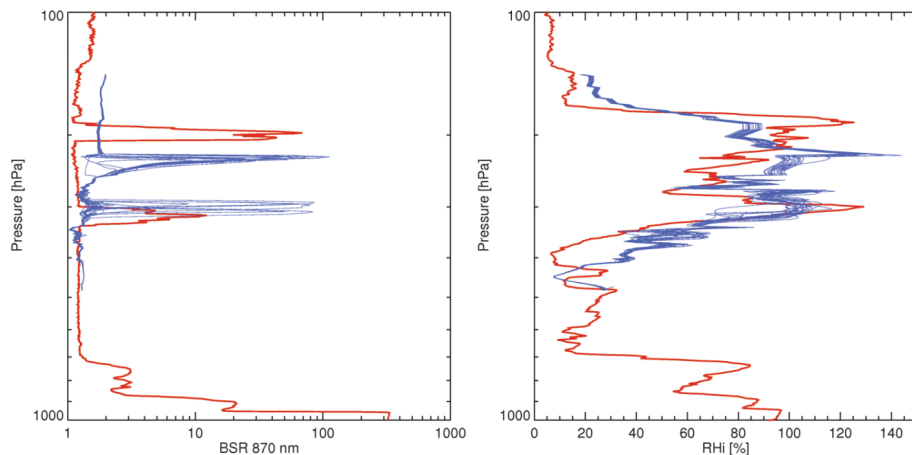


Fig. 6. All 20 microphysical column model runs (blue) with superimposed small-scale fluctuations compared with the measurements (red). The left panel shows BSR_{870} and the right RH_{ice} .

[Title Page](#)[Abstract](#)[Introduction](#)[Conclusions](#)[References](#)[Tables](#)[Figures](#)[◀](#)[▶](#)[◀](#)[▶](#)[Back](#)[Close](#)[Full Screen / Esc](#)[Printer-friendly Version](#)[Interactive Discussion](#)

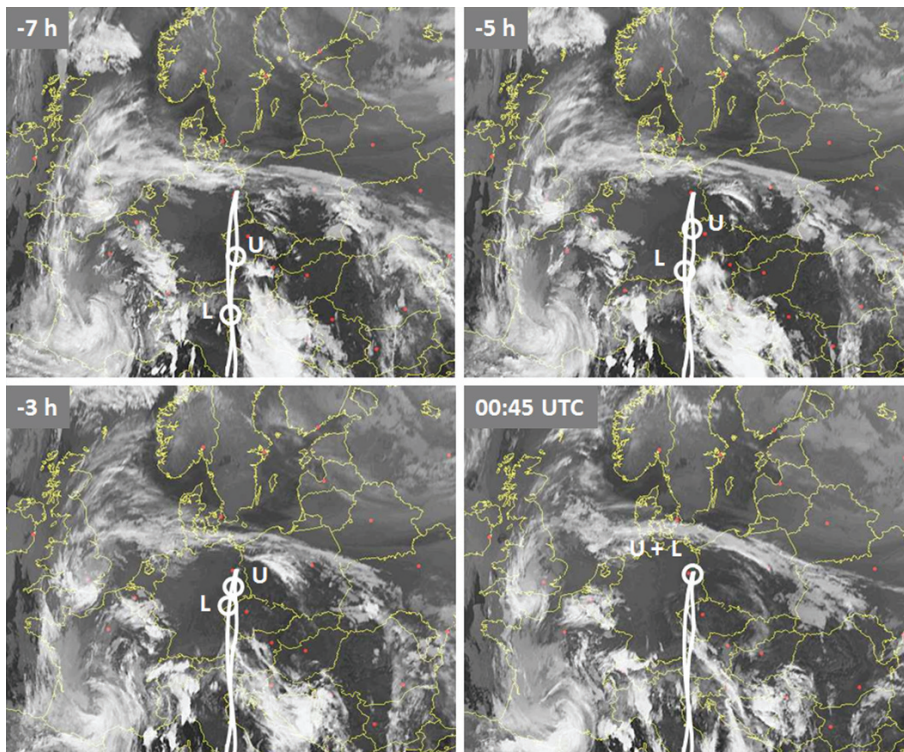


Fig. A1. Cloud images from the Meteosat satellite at four different times (Eumetsat, 2008). White lines: projections of the trajectories ending in the upper “U” and lower “L” cloud at 00:45 UTC. White circles: respective positions of air parcels 7 h, 5 h and 3 h upstream.

**Particle backscatter
and relative humidity**

M. Brabec et al.

Title Page	
Abstract	Introduction
Conclusions	References
Tables	Figures
◀	▶
◀	▶
Back	Close
Full Screen / Esc	
Printer-friendly Version	
Interactive Discussion	



Particle backscatter
and relative humidity

M. Brabec et al.

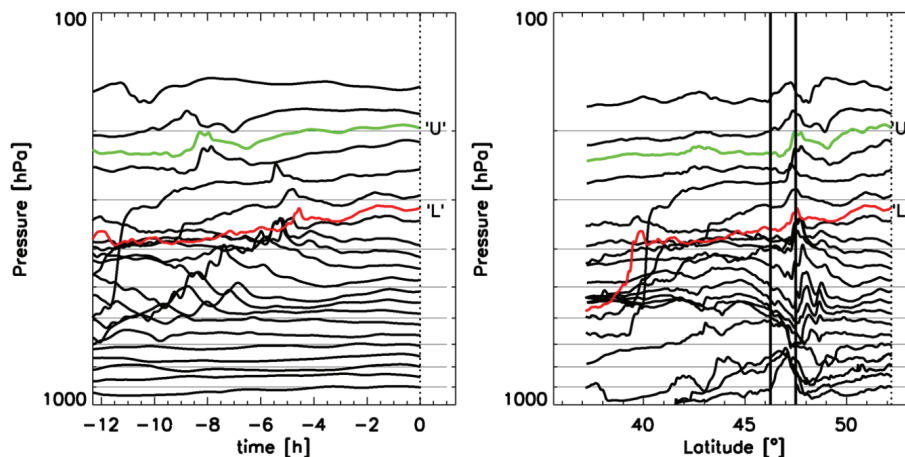


Fig. A2. Field of COSMO-7-based LAGRANTO trajectories highlighting the two trajectories ending in the lower cloud “L” (red) and upper cloud “U” (green). Left panel: trajectory pressure vs. time. Right panel: trajectory pressure vs. latitude. Waves are caused by the main chain of the Alps located around 47° N.

[Title Page](#)[Abstract](#)[Introduction](#)[Conclusions](#)[References](#)[Tables](#)[Figures](#)[◀](#)[▶](#)[◀](#)[▶](#)[Back](#)[Close](#)[Full Screen / Esc](#)[Printer-friendly Version](#)[Interactive Discussion](#)

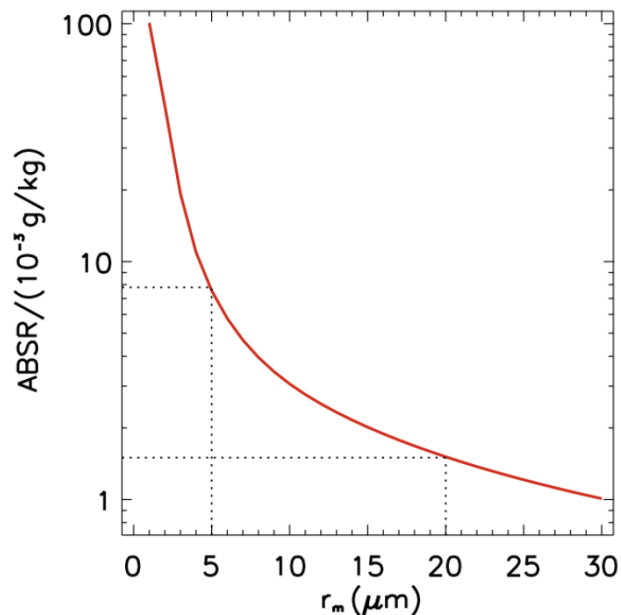


Fig. B1. Red curve: Simulated aerosol backscatter ratio (ABSR) at 870 nm wavelength per $10^{-3} \text{ g kg}^{-1}$ condensed as ice particles in a lognormal size distribution in dependence of the mode radius (r_m). The assumed conditions are a lognormal distribution width $\sigma = 1.4$, a refractive index of 1.31 (for ice), and an aspect ratio $A = 0.75$ for prolate spheroids as proxy for the ice particle asphericity. ABSR for IWC other than $10^{-3} \text{ g kg}^{-1}$ are obtained by appropriate scaling of the ordinate. Back dashed lines: typical range of r_m in high thin cirrus clouds (which formed in situ, e.g. by orographically forced upwelling), resulting in an overall uncertainty in BSR of a factor of ~ 4 .

Particle backscatter and relative humidity

M. Brabec et al.

Title Page	
Abstract	Introduction
Conclusions	References
Tables	Figures
◀	▶
◀	▶
Back	Close
Full Screen / Esc	
Printer-friendly Version	
Interactive Discussion	



Particle backscatter
and relative humidity

M. Brabec et al.

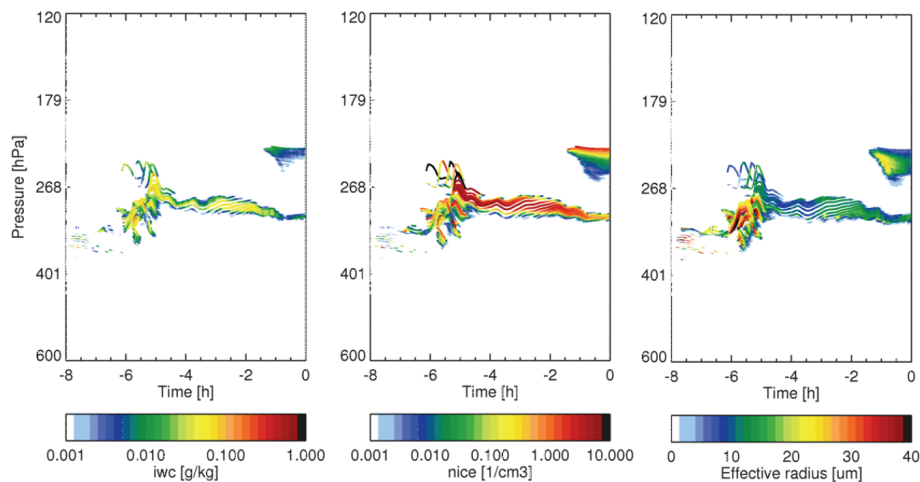


Fig. B2. Microphysical column model results for the case with superimposed small-scale temperature fluctuations showing additional parameters to Fig. 5. Left panel: ice water content, IWC. Center panel: ice number density, n_{ice} . Right panel: effective radius of the ice crystals, r_{eff} .

[Title Page](#)[Abstract](#)[Introduction](#)[Conclusions](#)[References](#)[Tables](#)[Figures](#)[◀](#)[▶](#)[◀](#)[▶](#)[Back](#)[Close](#)[Full Screen / Esc](#)[Printer-friendly Version](#)[Interactive Discussion](#)

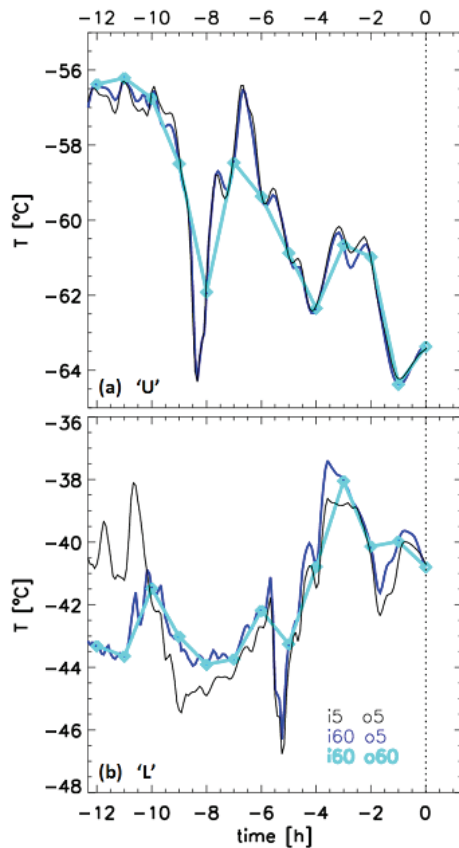


Fig. C1. Examples of backward trajectories for **(a)** the upper cloud “U”, **(b)** lower cloud “L”. Black curves: based on COSMO-7 fields with 5-min resolution, providing trajectory values every 5 min. Dark blue curves: based on COSMO-7 fields with 1-h resolution, interpolating trajectory values every 5 min. Cyan curves: based on COSMO-7 fields with 1-h resolution, providing trajectory values every 1 h.